High-Rate Scalable Entanglement Swapping Between Remote Entanglement Sources on Deployed New York City Fibers

Alexander N. Craddock,[1] Tyler Cowan,[2] Niccolò Bigagli,[1] Suresh Yekasiri,[3] Dylan Robinson,[1] Gabriel Bello Portmann,[1] Aditya Verma,[1] Ziyu Guo,[3] Michael Kilzer,[3] Jiapeng Zhao,[3] Mael Flament,[1] Javad Shabani,[2] Reza Nejabati,[3] and Mehdi Namazi[1,*]

[1]*Qunnect Inc., 141 Flushing Avenue, Suite 1110, Brooklyn, New York 11205-1005, USA*
[2]*Center for Quantum Information Physics, Department of Physics, New York University, New York 10003, USA*
[3]*Cisco Quantum Labs, Santa Monica, California 90404, USA*

(Received 17 April 2026; revised 13 July 2026; accepted 13 October 2026; published 10 November 2026)

Entanglement swapping between photon pairs generated at physically separated nodes over telecommunication fiber infrastructure is an essential step toward the quantum internet, enabling applications such as quantum repeaters, blind quantum computing, distributed quantum computing, and distributed quantum sensing. However, successful networked entanglement swapping relies on generating indistinguishable pairs of photons and preserving them over deployed fibers. This has limited most previous demonstrations to laboratory settings or relied on sophisticated methods to maintain the necessary indistinguishability. Here, we demonstrate a scalable entanglement-swapping experiment using naturally indistinguishable entanglement sources based on warm atomic vapor cells. Without sharing lasers or optical frequency references between nodes, nor the need for pulsing the sources, we achieve a swapping rate of nearly 500 pairs/s in a local configuration while maintaining the Clauser–Horne–Shimony–Holt (CHSH) parameter above 2. Additionally, we demonstrate the scalability of our method by maintaining the quality of the entanglement swapping on 17.6 km of deployed fibers in New York City, relying on commercially available single-photon avalanche detectors at the spoke nodes, superconducting nanowire detectors at the hub and standard time-synchronization techniques. Our work paves the way for the practical deployment of large-scale hub-and-spoke quantum networks within cities and data centers.

DOI: 10.1103/4xr6-2w3d

I. INTRODUCTION

Entanglement swapping is an important operation in the quantum internet [1], critical in use cases such as quantum repeaters [2], distributed quantum computing [3–5], and quantum sensing [6]. All such use cases require the entanglement-swapping process to be high-rate, stable, scalable, and deployable across telecommunication networks or within buildings, such as quantum data centers (QDCs) [7].

More specifically, entanglement swapping between remote photonic entanglement sources is not only crucial for creating long-distance quantum networks [8,9] but is also required for blind quantum computing [10,11] and enhancing the entanglement rate between quantum processors over a distributed quantum computing network [12]. However, while many groups have reported progress toward this goal in recent years, previous demonstrations have proven that efficient entanglement swapping between independent biphoton sources is a very hard task to achieve [13,14]. In addition, the deployment of such networks on the telecom infrastructure adds significant practical challenges.

One major challenge with swapping is the requirement of indistinguishability [15]. For this process to be successful, not only must the photons from different sources be identical to one another but also fiber effects, such as polarization drifts, must be mitigated to ensure high-fidelity entanglement swapping. With sources such as spontaneous parametric down-conversion (SPDC) [16], color centers in diamonds [17], and quantum dots [15], producing identical sources is a challenge. For sources that produce naturally indistinguishable photons, such as atomic and ionic systems, preserving the degrees of freedom of the photons across the network can be nontrivial [17,18].

Another challenge with entanglement swapping is achieving high rates. Since the operation relies on the

*Contact author: mehdi@quconn.com

Published by the American Physical Society under the terms of the Creative Commons Attribution 4.0 International license. Further distribution of this work must maintain attribution to the author(s) and the published article's title, journal citation, and DOI.

simultaneous arrival of photons from two different sources, probabilistic entanglement sources need to have high spectral brightness. To date, most experiments using such sources have resulted in rates below 1 event/s [13,14,19]. There are some exceptions, with the highest rate reported at 108 pairs/s [20], with similar swapping fidelity to that demonstrated here. Although impressive, this setup relied on two SPDC sources being pumped using the same laser, making it impractical to implement over a network. Deterministic sources, such as trapped ions or neutral atoms, do not necessarily have this timing issue because the photons can be made to arrive simultaneously. However, there are often issues with the collection efficiency of the photons and a lack of native telecom compatibility, which limits the distance over which swapping can be performed. Here, the highest rates achieved using such platforms reach a rate of 182 events/s at 422 nm, separated by roughly 2 m [21].

Here, we demonstrate entanglement swapping with polarization qubits that not only enables high-rate swapping but is also highly scalable for larger spoke-and-hub models, such as in QDCs and metropolitan networks. Using two fully independent, highly bichromatic atomic vapor-based entanglement sources, we achieve a swapping rate exceeding 470 pairs/s when the sources are "local" to the hub (all within the same building). The swapping is performed at telecom wavelengths and occurs at a superconducting nanowire-equipped hub, whereas the entangled photons are in the near infrared and detected with lower-cost SPADs. This architecture allows for the easy addition of more spokes, given the small size, weight, power, and cost requirements of the spoke equipment. Additionally, we demonstrate the scalability of our platform by performing the swapping experiment on 17.6 km of deployed fibers in New York City, placing the hub at a commercial data center, quantum to digital (QTD) systems. Using this layout, we achieve the first Hz-level polarization entanglement swapping over a commercially deployed network.

II. EXPERIMENTAL DETAILS

Figure 1 shows a hardware schematic for the two spokes (S1 and S2) and the hub (H) for the following experiments. The two spokes have identical layouts and are designed to be fully operational at room temperature. In contrast, the hub is equipped with superconducting nanowire detectors (SNSPDs) and therefore requires cryogenic cooling. This layout allows for a low-cost, low-maintenance expansion of the number of spoke nodes, all connected to the same central hub, without the need for any additional cryogenic SNSPDs.

At the spokes, there are fully independent entanglement sources based on spontaneous four-wave mixing in a warm rubidium vapor. Using a Qu-LSR to drive the vapor with 780-nm and 1367-nm pumps, the source generates bichromatic pairs of 795-nm and 1324-nm photons that are entangled in a $|\Phi_+\rangle = \frac{1}{\sqrt{2}}(|HH\rangle + |VV\rangle)$ Bell state [22]. In contrast to previous work, here the entanglement source utilizes an enriched rubidium-85 vapor as opposed to rubidium 87. This was done to provide biphotons that are more temporally compatible with off-the-shelf SPADs.

From the entanglement sources, the 795-nm photons pass through a free-space HWP followed by a polarizer, allowing us to perform CHSH-like measurements between the two spokes. Postpolarizer, 795-nm photons are coupled into fiber and directed toward a SPAD (detection efficiency ≈65%).

The 1324-nm photons are coupled into the fiber and directed toward the hub, where swapping occurs. At the hub, the 1324-nm photons from the two spokes are passed through a fiber-based BSM. This consists of a fiber-based 50:50 splitter followed by a pair of fiber-based polarizing beamsplitter (PBS) cubes. We use a set of paddles between the 50:50 splitter and one of the PBSs to allow us to orient the axes of the two PBSs in the BSM to be the same. The four output fibers of the BSM are coupled to the hub's SNSPDs (>80% and >93% detection efficiency for detectors when the hub is local and remote, respectively). The excess loss through the BSM setup is ≈1.3 dB and ≈1.9 for the local and networked experiments, respectively. The difference is related to some additional fiber optics that were required for remote control in the remote case and could be neglected in the future.

For the local experiments, the fibers used are relatively short and experience little polarization drift. As a result, active polarization compensation is unnecessary, so the Qu-APC is bypassed. For the city-wide experiment, we see fiber drift similar to previous experiments [23–25], and we similarly use the Qu-APC injector-compensator pair to stabilize the fibers to the hub. These devices operate as a pair and use time-division multiplexing, switching between the 1324-nm photons from the source and a classical laser at a similar wavelength to monitor the fiber and compensate for any polarization drifts that may have occurred. For the experiments shown, the Qu-APC was operated to check for polarization drifts every 30 s. When used, the uptime of the Qu-APC was in excess of 99% and added an insertion loss of ≈2 dB per link. In both experiments, a set of paddles is used on the fibers that go to the hub. These are used to correct for the polarization rotation experienced by the photons traveling down the fiber but are not adjusted during the experiments.

For both sets of experiments, data is collected from the various detectors using time-tagging devices local to those detectors. A classical network, utilizing a separate set of fibers from the ones that transmit the 1324-nm photons, allows data to be collated between the three locations using *TCP* and IP. We use the White Rabbit protocol to synchronize the time taggers at the three nodes, with the White Rabbit devices operating over the same fibers

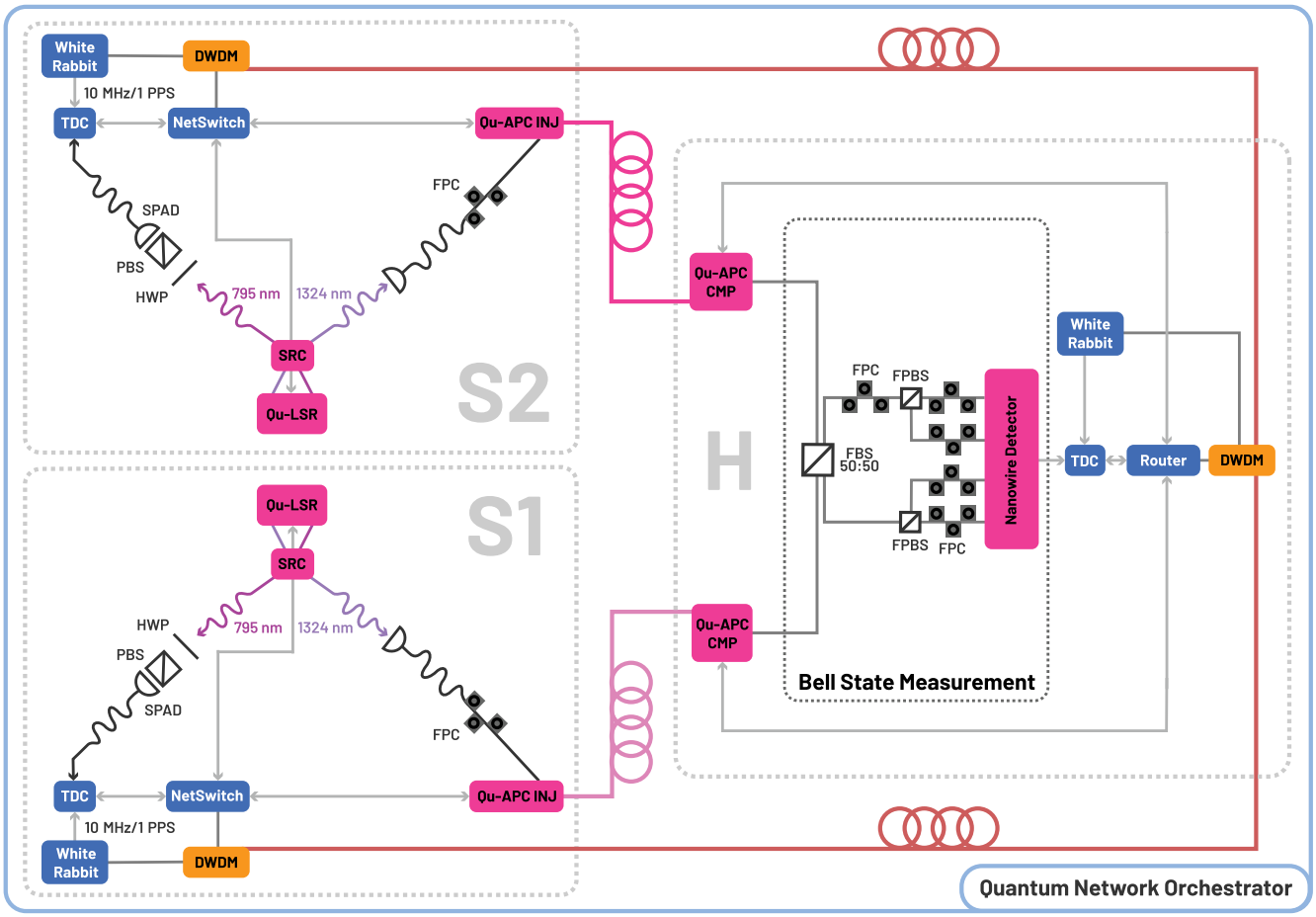


FIG. 1. Experimental layout of a three-node entanglement-swapping experiment. Nodes S1 and S2 host the independent entanglement sources, while H is where the entanglement swapping happens. Qu-LSR: Qunnect's dual-laser systems for the bichromatic sources. SRC: Atomic vapor cell sources. HWP: Half-wave plate. SPAD: Single-photon avalanche detector. TDC: Time-to-digital converter (time-tagging device). Qu-APC: Qunnect's automated polarization compensating devices (INJ: Injector. CMP: Compensator). FBS: Fiber beamsplitter. FPBS: Fiber polarization beamsplitter. All three nodes are controlled by Cisco's centralized quantum network orchestrator.

as the *TCP* and IP network. Cisco's quantum network orchestrator facilitates network operation by centrally controlling three experimental nodes. The integration of such an orchestrating software suite with the quantum layer is an essential step toward the expansion of such demonstrations to many-node configurations.

For both demonstrations, S1 and S2 are in two separate rooms (separated by ≈30 meters) of the same building at the Brooklyn Navy Yard in Brooklyn, New York. As mentioned above, the two rooms are fully fiber-gapped from each other. For the local experiments, the hub is colocated with S1. As such, the fiber loss from S1 to the hub is minimal, while the fiber loss from S2 to the hub is ≈1 dB.

For city-wide experiments, the hub is located in the historic 60 Hudson building in the QTD systems data center. The spokes are connected to the hub by fibers, shown in Fig. 2, of length ≈8.8 km, with a loss of ≈5 dB (measured by optical time-domain reflectometry at 1310 nm; the loss at 1324 nm is similar), bringing the combined fiber distance between S1 and S2 to ≈17.6 km.

III. LOCAL ENTANGLEMENT SWAPPING

As a benchmark of the swapping protocol between the independent sources, we first run the experiment with all the nodes located within the same building. Both entanglement sources are operated at a point where the peak cross-correlation function between the 795- and 1324-nm photons is ≈80. Here, the measured pair rate of the two sources at the detectors is ≈1.7 M/s and ≈1.3 M/s for S1 and S2, respectively, corresponding to a pair rate from the source of ≈4.1 and 4.0 M/s (the difference is attributed to slight fiber coupling differences between the sources). We optimize the paddles going from both S1 and S2 to the hub to ensure that the 1324-nm photons arriving at the hub's BSM are still in the state $|\Phi_+\rangle = \frac{1}{\sqrt{2}}(|HH\rangle + |VV\rangle)$ with the 795-nm photons at the spokes. For each set of angles

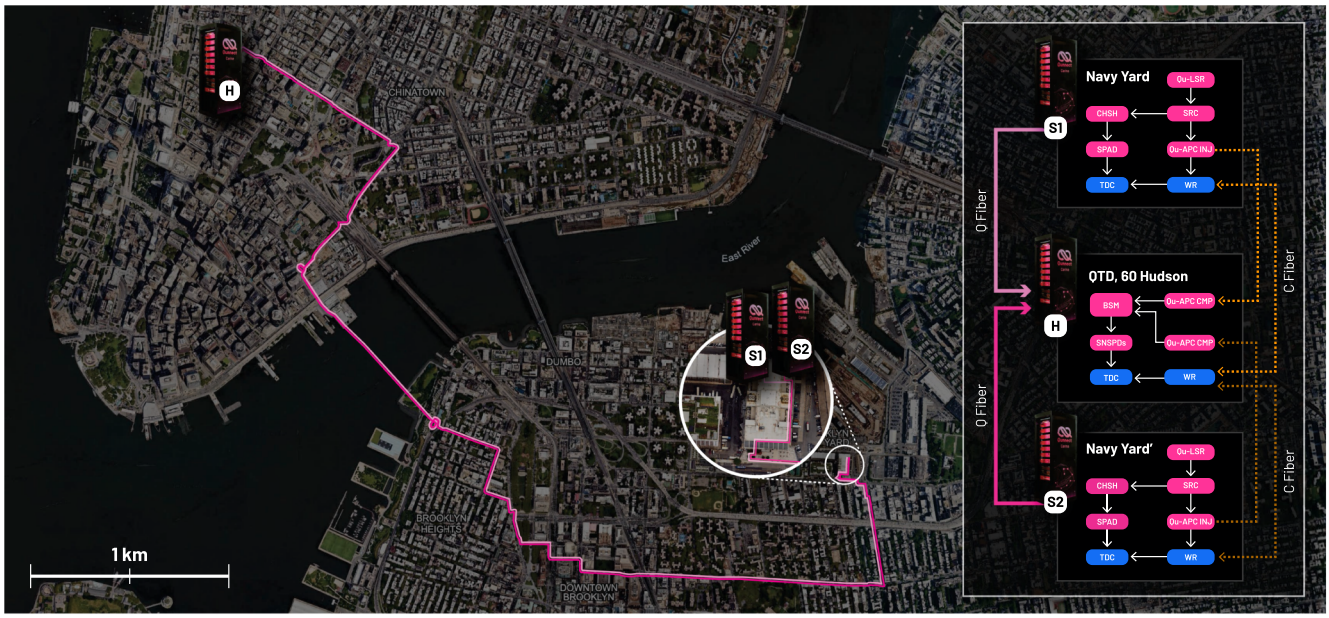


FIG. 2. Path of fibers for network experiments. Inset shows hardware used at the three locations. WR: White Rabbit, TDC: time-tagging device, SPAD: single-photon avalanche detector, SNSPD: superconducting nanowire single-photon detector, Qu-LSR: Qunnect dual-laser pump system, SRC: Entanglement source, CHSH: apparatus for performing CHSH-type measurements, SWAP: Bell state measurement (BSM) optics for swapping, and Qu-APC: Qunnect's automated polarization compensating device.

for the spoke HWP's, we record the relevant fourfold coincidences for 60 s.

Figures 3(a) and 3(b) show the fourfold coincidences vary as a function of the wave plate angles at S1 and S2 for one of the heralded Bell states. We observe the interference fringes typical of a polarization-entangled pair of photons. We note here that the differing visibility for the curves in panels (a) and (b) is expected for our system. For panel (a), the visibility is limited only by the effective cross-correlation (the cross-correlation averaged over the region of interest used for coincidence measurements) of the entanglement sources. For panel (b), the visibility is limited by the cross-correlation of the sources and the Hong-Ou-Mandel visibility of the sources (≈80% for the data shown in Fig. 3).

In Fig. 3(c), we reanalyze the collected data using different regions of interest for the fourfold coincidence. We show the relationship between the swapping fidelity (using the Bell S parameter as a proxy) and the measured swapping rate. As can be seen, $S > 2$ for the measured swapping rates exceeding 200/s. Accounting for the SPADs' detection efficiency of 65%, our measurement corresponds to an entanglement-swapping rate in excess of 470/s. Achieving high rates using fully independent entanglement sources paves the path toward deployed quantum repeaters and hybrid distributed quantum computing systems.

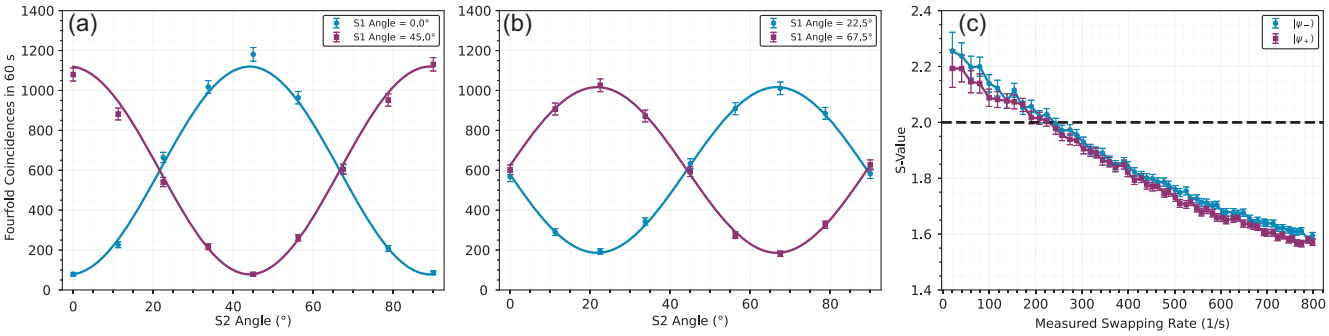


FIG. 3. Experimental results for the local swapping experiment. Panels (a) and (b) show interference fringes as the HWP at S1 and S2 are rotated. From the data, we extract Bell's S parameter and the swapping rate. We do this many times, changing the region of interest used for analysis to obtain the plot in panel (c) of the S parameter as a function of the swapping rate.

IV. ENTANGLEMENT SWAPPING OVER DEPLOYED NEW YORK CITY FIBERS

Next, we demonstrate entanglement swapping over deployed fiber in New York City. As discussed, here the hub is connected to the spokes by ≈8.8 km of fiber, with the fiber route shown in Fig. 2. We operate the sources in the same configuration used for the local experiments, where the peak measured cross-correlation is ≈80. Due to the increased losses from the spokes to the hub, we see lower pair rates of ≈240 k/s and ≈180 k/s for S1 and S2, respectively. Given that the sources operate nearly identically to the local experiment, we estimate an additional loss of 8.3 and 8.6 dB for S1 and S2. Taking into account the difference in detection efficiency between the experiments and the differing loss in the BSM (used in these measurements), this corresponds to a link loss of ≈8.2 and ≈9.5 dB for the S1-hub and S2-hub links, respectively. We independently measure losses of ≈7 dB for the deployed fiber (≈5 dB for the fiber itself and ≈2 dB for the Qu-APC), and we attribute the additional loss to those incurred in connecting the equipment at the spokes and hub to the deployed fiber due to patch panels and connectors.

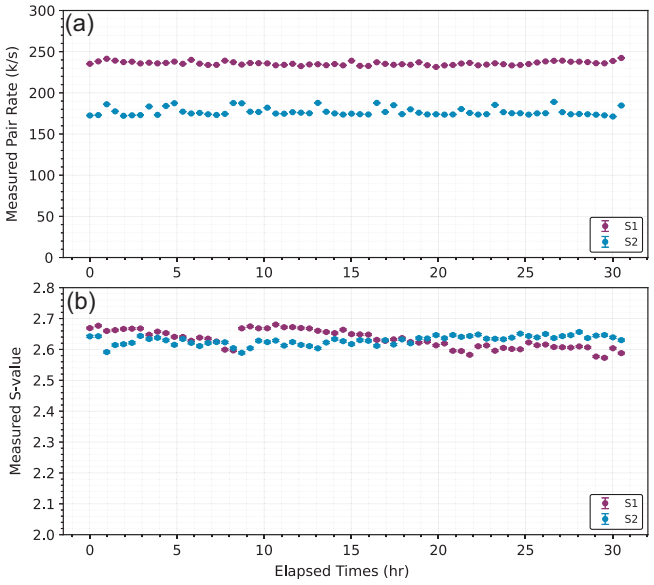


FIG. 4. Single-spoke entanglement distribution stability results. Panel (a) shows the measured pair rate and panel (b) shows the entanglement fidelity, parametrized by the Bell's S parameter, as a function of time.

For this experiment, we again optimize the paddles so that the 1324- and 795-nm photons of both spokes are in the $|\Phi_+\rangle = \frac{1}{\sqrt{2}}(|HH\rangle + |VV\rangle)$ state after fiber propagation. We operate the Qu-APC to check the fiber drift every 30 s and perform corrections if necessary.

Before performing the swapping experiment, we first check the stability of the single-fiber entanglement distribution. As shown in Fig. 4(a), the measured pair rate through the network is stable to ±5% over 30 h. More importantly than the pair rate, for entanglement swapping over the deployed fiber to be successful, we require that the fidelity of the entanglement generated at the two spokes is preserved upon arriving at the hub. To this end, we also monitor the Bell S parameter over the same 30-hr period for the two individual sources and observe relatively stable behavior, as demonstrated in Fig. 4(b). We note that the Qu-APC has some programmed tolerance threshold for allowable fiber drift before it compensates. Therefore, some small drift, such as that shown in the figure, is expected.

Having established the stability of the network, we move on to demonstrate entanglement swapping using the deployed fibers. As in the local experiment, we again set the HWPs at the two spokes to defined angles before accumulating data for 60 s. We cycle through each set of HWP angles 20 times so that each angle pair has data recorded for 1200 s. Although we have noticed that the entanglement distribution through the network is relatively stable, we perform this method of data accumulation to spread the effect of any small fluctuations in either the source rate or fiber polarization drift over all the angle pairs, so as not to bias the results. As we rotate the HWPs, we again observe characteristic interference fringes consistent with polarization-entangled photon pairs, as shown in Figs. 5(a) and 5(b).

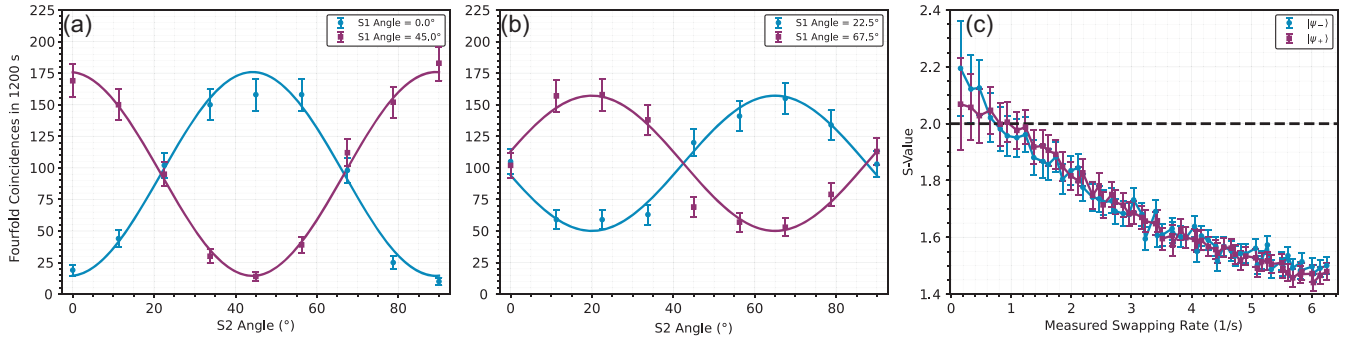


FIG. 5. Experimental results for the network swapping experiment. Panels (a) and (b) show interference fringes as the HWP at S1 and S2 are rotated. From the data, we extract Bell's S parameter and the swapping rate. We do this many times, changing the region of interest used for analysis to obtain the plot in panel (c) of the S parameter as a function of the swapping rate.

Similar to the local data, we reanalyze the swapping data using different regions of interest to examine the relationship between the swapping rate and fidelity, the results of which are shown in Fig. 5(c). We observe values of $S > 2$ for measured swapping rates over 0.65/s. Accounting for the SPADs' detection efficiency of 65%, our measurement corresponds to an entanglement-swapping rate in excess of 1.5/s.

V. DISCUSSION AND CONCLUSION

High-rate, field-deployable entanglement swapping is an important step in the development of the quantum internet. Here, we have demonstrated entanglement swapping in both a local setting and over a deployed 17.6-km network on GothamQ, New York City. We show that by adjusting the bin width used in the analysis, we increase the swapping rate at the expense of reducing the entanglement-swapping fidelity, which we parameterize by Bell's S parameter. In the local setting, we observe swapping rates exceeding 470/s while maintaining $S > 2$, whereas over the deployed network the rate is in excess of 1.5/s.

There are many near- and long-term applications for scalable, deployed entanglement swapping. For metropolitan scales, an important example is the use of swapping to improve the practical security of entanglement-based quantum encryption protocols [26]. While these protocols are naturally source independent, entanglement swapping adds the measurement device independent layer, bringing the deployment much closer to full device independent quantum key distribution (QKD) [27,28]. In the current implementation, the achieved rates are likely too low for practical implementation of device independent quantum key distribution (DIQKD). However, with improvements to the heralding efficiency of the entanglement source (≈20%), a reduction in the detection losses (of order 1–2 dB for each photon), and losses in the Qu-APC (≈2 dB for each fiber), we believe several orders of magnitude increase in swapping rate are possible. A similar application for which there are potential near-term applications is bit commitment quantum position verification [29]. In these protocols, entanglement swapping and/or teleportation act as an equivalent of a quantum nondemolishing measurement, allowing for the parties to validate the arrival of photons without measuring them. For the purposes of quantum repeating, the requirements on the fidelity are less stringent. With the current system rates over 10^3/s "locally" and 10/s in the deployed setting are currently attainable, while still being of sufficient fidelity to perform entanglement purification [30]. Similarly, improvements to the system could increase the rates by orders of magnitude.

In most swapping experiments with paired sources, the photons used are near degenerate. Therefore, we emphasize the use of atomic-based bichromatic entanglement sources in this work. Not only do these sources eliminate the need for using cryogenic detectors or input laser sharing, but they also remove the need for frequency conversion in many quantum repeating and distributed protocols. The newly entangled 795-nm (or 780-nm) photons over the telecommunication network are natively compatible with a large variety of quantum memories, neutral atom quantum computers, atomic clocks, and quantum sensors. More importantly, we deploy a scalable "spoke-and-hub" network in which the spokes do not require any sophisticated or cryogenically cooled technology, including the single-photon detectors. Such an architecture is essential for scaling networks within cities or QDCs.

Finally, large-scale quantum networks require both scalable hardware and software to work seamlessly together. Bringing together Qunnect's Carina system with Cisco's orchestrator software for a quantum networking operation at one of Manhattan's busiest data centers aims to demonstrate the readiness of quantum entanglement networks for industrial deployments beyond point-to-point use cases.

ACKNOWLEDGMENTS

We would like to sincerely thank QTD Systems LLC, especially Peter Feldman, for not only accommodating our hardware at their data center but also for providing seamless access and the partnership necessary for a first-of-its-kind quantum experiment. Additionally, a major thank you to Vijoy Pandey and Ramana Kompella of Cisco and Noel Goddard of Qunnect, without whom this collaboration would not have been possible.

DATA AVAILABILITY

The data that support the findings of this article are not publicly available because they contain commercially sensitive information. The data are available from the authors upon reasonable request.

[1] H. J. Kimble, *The quantum internet*, Nature (London) **453**, 1023 (2008).

[2] K. Azuma, S. E. Economou, D. Elkouss, P. Hilaire, L. Jiang, H.-K. Lo, and I. Tzitrin, *Quantum repeaters: From quantum networks to the quantum internet*, Rev. Mod. Phys. **95** 045006 (2023).

[3] C. Monroe, R. Raussendorf, A. Ruthven, K. R. Brown, P. Maunz, L.-M. Duan, and J. Kim, *Large-scale modular quantum-computer architecture with atomic memory and photonic interconnects*, Phys. Rev. A **89**, 022317 (2014).

[4] S. Pirandola and S. L. Braunstein, *Physics: Unite to build a quantum internet*, Nature (London) **532**, 169 (2016).

[5] S. Wehner, D. Elkouss, and R. Hanson, *Quantum internet: A vision for the road ahead*, Science **362**, eaam9288 (2018).

[6] E. T. Khabiboulline, J. Borregaard, K. De Greve, and M. D. Lukin, *Optical interferometry with quantum networks*, Phys. Rev. Lett. **123**, 070504 (2019).

[7] E. Shchukin and P. van Loock, *Optimal entanglement swapping in quantum repeaters*, Phys. Rev. Lett. **128**, 150502 (2022).
[8] R. Kaltenbaek, R. Prevedel, M. Aspelmeyer, and A. Zeilinger, *High-fidelity entanglement swapping with fully independent sources*, Phys. Rev. A **79**, 040302(R) (2009).
[9] N. Sangouard, C. Simon, B. Zhao, Y.-A. Chen, H. de Riedmatten, J.-W. Pan, and N. Gisin, *Robust and efficient quantum repeaters with atomic ensembles and linear optics*, Phys. Rev. A **77**, 062301 (2008).
[10] A. Broadbent, J. Fitzsimons, and E. Kashefi, *Universal blind quantum computation*, in *2009 50th Annual IEEE Symposium on Foundations of Computer Science* (IEEE, NW Washington, DC, United States 2009).
[11] Q. Li, W. H. Chan, C. Wu, and Z. Wen, *Triple-server blind quantum computation using entanglement swapping*, Phys. Rev. A **89**, 040302(R) (2014).
[12] H. Shapourian, E. Kaur, T. Sewell, J. Zhao, M. Kilzer, R. Kompella, and R. Nejabati, *Quantum data center infrastructures: A scalable architectural design perspective*, arXiv:2501.05598.
[13] S. I. Davis, R. Valivarthi, A. Cameron, C. Pena, S. Xie, L. Narvaez, N. Lauk, C. Li, K. Taylor, R. Youssef, C. Wang, K. Kapoor, B. Korzh, N. Sinclair, M. Shaw, P. Spentzouris, and M. Spiropulu, *Entanglement swapping systems toward a quantum internet*, arXiv:2503.18906.
[14] Q.-C. Sun, Y.-F. Jiang, Y.-L. Mao, L.-X. You, W. Zhang, W.-J. Zhang, X. Jiang, T.-Y. Chen, H. Li, Y.-D. Huang, X.-F. Chen, Z. Wang, J. Fan, Q. Zhang, and J.-W. Pan, *Entanglement swapping over 100 km optical fiber with independent entangled photon-pair sources*, Optica **4**, 1214 (2017).
[15] F. Basso Basset, M. B. Rota, C. Schimpf, D. Tedeschi, K. D. Zeuner, S. F. Covre da Silva, M. Reindl, V. Zwiller, K. D. Jöns, A. Rastelli, and R. Trotta, *Entanglement swapping with photons generated on demand by a quantum dot*, Phys. Rev. Lett. **123**, 160501 (2019).
[16] J.-W. Pan, D. Bouwmeester, H. Weinfurter, and A. Zeilinger, *Experimental entanglement swapping: Entangling photons that never interacted*, Phys. Rev. Lett. **80**, 3891 (1998).
[17] A. J. Stolk *et al.*, *Metropolitan-scale heralded entanglement of solid-state qubits*, Sci. Adv. **10**, eadp6442 (2024).
[18] W.-Z. Liu *et al.*, *Long-lived remote ion-ion entanglement for scalable quantum repeaters*, Nature (London) **652**, 51 (2026).
[19] J. Park, H. Kim, and H. Seb Moon, *Entanglement swapping with autonomous polarization-entangled photon pairs from a warm atomic ensemble*, Opt. Lett. **45**, 2403 (2020).
[20] R.-B. Jin, M. Takeoka, U. Takagi, R. Shimizu, and M. Sasaki, *Highly efficient entanglement swapping and teleportation at telecom wavelength*, Sci. Rep. **5**, 9333 (2015).
[21] L. J. Stephenson, D. P. Nadlinger, B. C. Nichol, S. An, P. Drmota, T. G. Ballance, K. Thirumalai, J. F. Goodwin, D. M. Lucas, and C. J. Ballance, *High-rate, high-fidelity entanglement of qubits across an elementary quantum network*, Phys. Rev. Lett. **124**, 110501 (2020).
[22] A. N. Craddock, Y. Wang, F. Giraldo, R. Sekelsky, M. Flament, and M. Namazi, *High-rate subgigahertz-linewidth bichromatic entanglement source for quantum networking*, Phys. Rev. Appl. **21**, 034012 (2024).
[23] A. N. Craddock, A. Lazenby, G. B. Portmann, R. Sekelsky, M. Flament, and M. Namazi, *Automated distribution of polarization-entangled photons using deployed New York City fibers*, PRX Quantum **5**, 030330 (2024).
[24] M. Sena, M. Flament, S. Andrewski, I. Caltzidis, N. Bigagli, T. Rieser, G. Bello Portmann, R. Sekelsky, R.-P. Braun, A. N. Craddock, M. Schulz, K. D. Jöns, M. Ritter, M. Geitz, O. Holschke, and M. Namazi, *High-fidelity quantum entanglement distribution in metropolitan fiber networks with co-propagating classical traffic*, J. Opt. Commun. Netw. **17**, 1072 (2025).
[25] Y. Shi, J. Su, A. Rahmouni, P. Shrestha, M. Merzouki, G. B. Portmann, A. Lazenby, M. Flament, M. Namazi, A. Battou, O. Slattery, and T. Gerrits, *Entanglement distribution over a polarization-stabilized aerial fiber*, arXiv:2601.11753.
[26] D. Mayers and A. Yao, *Quantum cryptography with imperfect apparatus*, in *Proceedings 39th Annual Symposium on Foundations of Computer Science (Cat. No.98CB36280)*, Palo Alto, CA, USA (1998), pp. 503–509, https://ieeexplore.ieee.org/xpl/conhome/5965/proceeding.
[27] Z. Ye-Qi and X. Jing-Bo, *Entanglement swapping of pair coherent states with phase decoherence*, Chin. Phys. Lett. **26**, 070301 (2009).
[28] S. Vijayaraj and M. Paternostro, *Improving device-independent quantum key distribution protocols through multiple routed bell tests*, arXiv:2606.26329.
[29] L. Escolà-Farràs, B. Škorić, and F. Speelman, *Arbitrarily loss-tolerant quantum position verification in a single execution*, arXiv:2606.25037.
[30] C. H. Bennett, G. Brassard, S. Popescu, B. Schumacher, J. A. Smolin, and W. K. Wootters, *Purification of noisy entanglement and faithful teleportation via noisy channels*, Phys. Rev. Lett. **76**, 722 (1996).